

Spin Excitation Anisotropy as a Probe of Orbital Ordering in the Paramagnetic Tetragonal Phase of Superconducting $\text{BaFe}_{1.904}\text{Ni}_{0.096}\text{As}_2$

Huiqian Luo,¹ Meng Wang,¹ Chenglin Zhang,^{2,3} Xingye Lu,¹ Louis-Pierre Regnault,⁴ Rui Zhang,¹ Shiliang Li,¹ Jiangping Hu,^{1,5} and Pengcheng Dai^{2,3,1,*}

¹*Beijing National Laboratory for Condensed Matter Physics, Institute of Physics, Chinese Academy of Sciences, Beijing 100190, China*

²*Department of Physics and Astronomy, Rice University, Houston, Texas 77005, USA*

³*Department of Physics and Astronomy, The University of Tennessee, Knoxville, Tennessee 37996-1200, USA*

⁴*SPSMS-MDN, UMR-E CEA/UJF-Grenoble 1, INAC, Grenoble, F-38054, France*

⁵*Department of Physics, Purdue University, West Lafayette, Indiana 47907, USA*

(Received 27 January 2013; published 5 September 2013)

We use polarized neutron scattering to demonstrate that in-plane spin excitations in electron doped superconducting $\text{BaFe}_{1.904}\text{Ni}_{0.096}\text{As}_2$ ($T_c = 19.8$ K) change from isotropic to anisotropic in the tetragonal phase well above the antiferromagnetic (AFM) ordering and tetragonal-to-orthorhombic lattice distortion temperatures ($T_N \approx T_s = 33 \pm 2$ K) without an uniaxial pressure. While the anisotropic spin excitations are not sensitive to the AFM order and tetragonal-to-orthorhombic lattice distortion, superconductivity induces further anisotropy for spin excitations along the $[110]$ and $[\bar{1}\bar{1}0]$ directions. These results indicate that the spin excitation anisotropy is a probe of the electronic anisotropy or orbital ordering in the tetragonal phase of iron pnictides.

DOI: [10.1103/PhysRevLett.111.107006](https://doi.org/10.1103/PhysRevLett.111.107006)

PACS numbers: 74.70.Xa, 75.30.Gw, 78.70.Nx

Understanding the electronic anisotropic state (electronic nematicity) at a temperature associated with the pseudogap phase is one of the most important unresolved problems in the quest for mechanism of high- T_c superconductivity in copper oxides [1]. For iron pnictide superconductors derived from electron doping to their antiferromagnetic (AFM) parent compounds [2–4], there is considerable evidence for an anisotropic electronic state in the AFM phase with an orthorhombic lattice distortion [5–7]. Upon warming to above the AFM order (T_N) and orthorhombic lattice distortion (T_s) temperatures, iron pnictide superconductors become paramagnetic tetragonal metals [4]. Although transport [8], resonant ultrasound [9], angle-resolved photoemission spectroscopy (ARPES) [10], neutron scattering [11], and magnetic torque [12] measurements suggest an electronic anisotropy in the paramagnetic tetragonal phase, much is unclear about its microscopic origin. In one class of models, the observed electronic anisotropy in the paramagnetic tetragonal phase of iron pnictides [8–12] may arise from either in-plane spin anisotropy (spin nematic phase) [13] as suggested from magnetic anisotropy in torque measurements [12], or orbital ordering [14–19] as implied from the energy splitting of the d_{xz} - and d_{yz} -dominated bands above T_N in ARPES [10]. However, there is no sufficient experimental evidence for spin nematic phase [20] and the observed orbital anisotropy in ARPES [10] may also be an extrinsic effect due to an uniaxial pressure induced increase in T_N [21]. Instead of an electronic anisotropic spin nematic state or orbital ordering, the large resistivity anisotropy seen in electron-doped $\text{BaFe}_{2-x}\text{Co}_x\text{As}_2$ [8] has been interpreted as being

due to anisotropic impurity scattering of Co atoms in the FeAs layer [22,23]. Since the in-plane resistivity anisotropy in charge transport property does not directly couple to spin and orbital order, these experimental results still leave open the question concerning the presence of spin nematicity or orbital ordering in the tetragonal phase of iron pnictides [13–19].

Here we use polarized neutron scattering to study the spin anisotropy in electron-doped iron pnictide superconductor $\text{BaFe}_{1.904}\text{Ni}_{0.096}\text{As}_2$ ($T_c = 19.8$ K) [24]. This material has incommensurate AFM order (T_N) and tetragonal-to-orthorhombic lattice distortion (T_s) temperatures below $T_N \approx T_s = 33 \pm 2$ K (Fig. 1) [25]. Since the spin anisotropy in iron pnictide must originate from a spin-orbit coupling [26], its temperature dependence can provide direct information on any change of electronic physics involving spin or orbital degree of freedom. We demonstrate that spin excitations in $\text{BaFe}_{1.904}\text{Ni}_{0.096}\text{As}_2$ exhibit an in-plane isotropic to anisotropic transition in the tetragonal phase at a temperature corresponding to the onset of in-plane resistivity anisotropy [8]. While the spin anisotropy shows no anomaly across T_N and T_s , it enhances dramatically below T_c revealing its connection to superconductivity. Since similar spin anisotropy is only observed in the AFM orthorhombic phase of the undoped BaFe_2As_2 [27], spin-orbit coupling in the paramagnetic tetragonal phase of $\text{BaFe}_{1.904}\text{Ni}_{0.096}\text{As}_2$ must be stabilized by an electronic anisotropic (nematic) phase or orbital ordering.

Figure 1(a) shows the schematic electronic phase diagram of $\text{BaFe}_{2-x}\text{Ni}_x\text{As}_2$ as determined from neutron scattering [24] and transport measurements [28,29]. In the

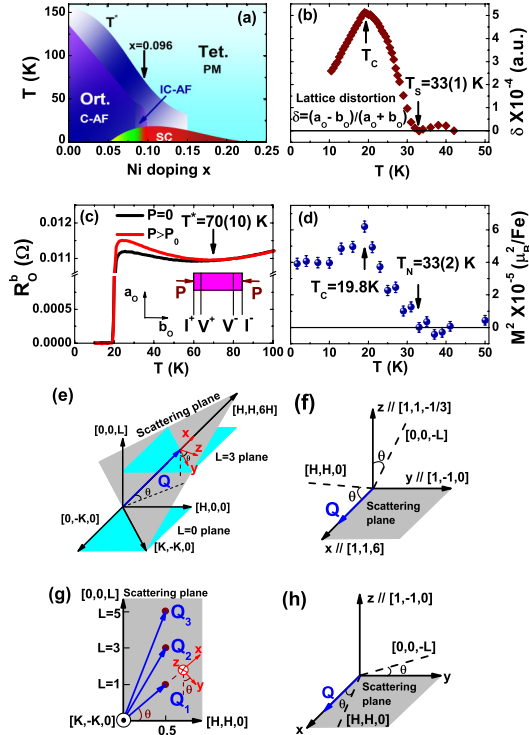


FIG. 1 (color online). (a) Electronic phase diagram of $\text{BaFe}_{2-x}\text{Ni}_x\text{As}_2$ as a function of Ni doping x , where T^* is the zone boundary of anisotropic in-plane resistivity obtained from Ref. [29]. The arrow indicates the doping level $x = 0.096$ for our experiments. (b) Orthorhombic lattice distortion order parameter δ shows $T_s = 33 \pm 1$ K. The high resolution x-ray diffraction on nuclear peak (2, 2, 12) experiment was from Ref. [25]. (c) In-plane resistance under zero and finite uniaxial stress P along b_o , where $P = P_0$ is the detwinned pressure. From separate neutron scattering measurements, we know that T_N and T_s are uniaxial stress independent. (d) Temperature dependence of the AFM order parameter shows $T_N = 33 \pm 2$ K. (e),(g) Scattering plane and neutron polarization directions in our experiments. (f),(h) Magnetic response of SF channels in the neutron polarization analysis.

tetragonal phase above the T_N and T_s , transport measurements show anisotropic resistivity along the orthorhombic a_o and b_o directions below the electronic nematic ordering temperature T^* [8]. We chose to study $\text{BaFe}_{1.904}\text{Ni}_{0.096}\text{As}_2$ because this sample has coexisting short-range incommensurate AFM order and superconductivity [24]. From previous high-resolution x-ray diffraction experiments on $\text{BaFe}_{2-x}\text{Co}_x\text{As}_2$ [30] and $\text{BaFe}_{2-x}\text{Ni}_x\text{As}_2$ [25], we know that $\text{BaFe}_{1.904}\text{Ni}_{0.096}\text{As}_2$ changes from tetragonal to orthorhombic lattice structure below T_s , and the lattice orthorhombicity becomes smaller on entering the superconducting state. Figure 1(b) shows the temperature dependence of orthorhombicity $\delta = (a_o - b_o)/(a_o + b_o)$, revealing $T_s = 33 \pm 1$ K [25]. Although the orthorhombicity of the system clearly decreases on cooling below T_c , its lattice structure does not become fully tetragonal at 10 K [Fig. 1(b)]. Similarly, temperature dependence of

the magnetic order parameter indicates a Néel temperature of $T_N = 33 \pm 2$ K [Fig. 1(d)] [24]. To confirm the anisotropic resistivity in the tetragonal phase of $\text{BaFe}_{1.904}\text{Ni}_{0.096}\text{As}_2$, we have also carried out resistivity measurements on a detwinned sample. The outcome shows clear resistivity anisotropy for temperatures below $T^* = 70 \pm 10$ K [Fig. 1(c)].

We prepared sizable high quality single crystals of $\text{BaFe}_{1.904}\text{Ni}_{0.096}\text{As}_2$ using the self-flux method [28] and coaligned ~ 11 g single crystals within 3° full width at half maximum (FWHM). Our polarized neutron scattering experiments were carried out using the IN22 thermal triple-axis spectrometer at the Institut Laue-Langevin, Grenoble, France [26]. The scattering planes are $(H, H, 6H) \times (K, -K, 0)$ and $(H, H, 0) \times (0, 0, L)$ to probe the wave vector dependence of spin excitations along different directions. Using pseudotetragonal lattice unit cell with $a \approx b \approx 3.956$ Å, and $c = 12.92$ Å, the vector \mathbf{Q} in three-dimensional reciprocal space in Å⁻¹ is defined as $\mathbf{Q} = H\mathbf{a}^* + K\mathbf{b}^* + L\mathbf{c}^*$, where H, K , and L are Miller indices and $\mathbf{a}^* = \hat{\mathbf{a}}2\pi/a$, $\mathbf{b}^* = \hat{\mathbf{b}}2\pi/b$, $\mathbf{c}^* = \hat{\mathbf{c}}2\pi/c$ are reciprocal lattice units. We define neutron polarization directions as x, y, z , with x parallel to \mathbf{Q} , y and z perpendicular to \mathbf{Q} as shown in Figs. 1(e) and 1(g). At the AFM wave vector $\mathbf{Q} = (0.5, 0.5, 3)$, neutron polarization directions x and y are parallel to the $\mathbf{Q} = (1, 1, 6)$ and $(1, -1, 0)$ respectively, while z is perpendicular to the $(H, H, 6H) \times (K, -K, 0)$ scattering plane along the $\mathbf{Q} = (1, 1, -1/3)$ direction [Figs. 1(e) and 1(f)]. In the (H, H, L) scattering plane, we probe AFM wave vectors $\mathbf{Q}_1 = (0.5, 0.5, 1)$, $\mathbf{Q}_2 = (0.5, 0.5, 3)$, $\mathbf{Q}_3 = (0.5, 0.5, 5)$, where neutron polarization directions x, y , and z are shown in Fig. 1(g).

Since neutron scattering is only sensitive to magnetic scattering component perpendicular to the momentum transfer \mathbf{Q} , magnetic responses within the y - z plane (M_y and M_z) can be measured by using different neutron spin directions [Figs. 1(f) and 1(h)]. At a specific momentum and energy transfer, scattered neutrons can have polarizations antiparallel (neutron spin flip or SF, $\uparrow\downarrow$) to the incident neutrons. Therefore, the three neutron SF scattering cross sections can be written as $\sigma_\alpha^{\text{SF}}$, where $\alpha = x, y, z$. The magnetic moments M_y and M_z can be extracted via $\sigma_x^{\text{SF}} - \sigma_y^{\text{SF}} = cM_y$ and $\sigma_x^{\text{SF}} - \sigma_z^{\text{SF}} = cM_z$, where $c = (R - 1)/(R + 1)$ and the flipping ratio R is measured by the leakage of non-spin-flip (NSF) nuclear Bragg peaks into the magnetic SF channel $R = \sigma_{\text{Bragg}}^{\text{NSF}}/\sigma_{\text{Bragg}}^{\text{SF}} \approx 15$ [26].

In previous polarized neutron scattering experiments on optimally electron-doped iron pnictide superconductor $\text{BaFe}_{1.9}\text{Ni}_{0.1}\text{As}_2$ [26] and $\text{BaFe}_{1.88}\text{Co}_{0.12}\text{As}_2$ [31] without static AFM order, low-energy spin excitations were found to be anisotropic in the superconducting state. For electron-overdoped $\text{BaFe}_{1.85}\text{Ni}_{0.15}\text{As}_2$, spin excitations are isotropic in both the normal and superconducting states [32].

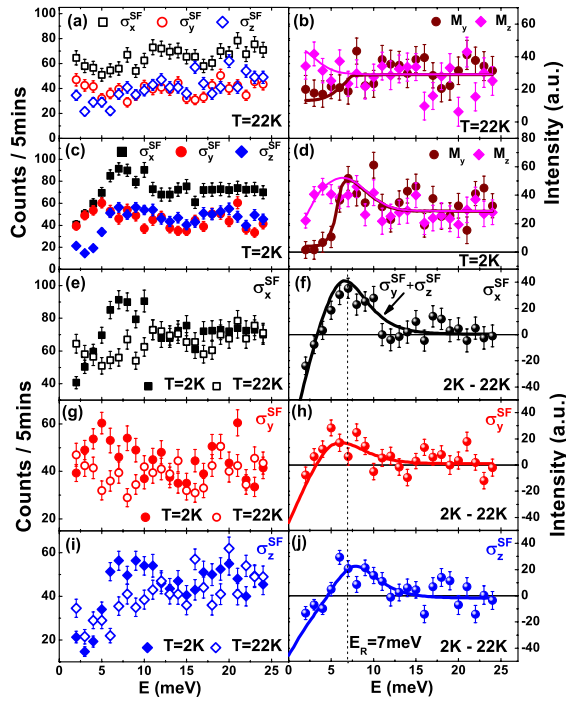


FIG. 2 (color online). (a) Energy scans at $\mathbf{Q} = (0.5, 0.5, 3)$ for SF scattering at 22 K above T_c for different neutron polarization directions, marked as $\sigma_{x,y,z}^{\text{SF}}$. (b) The magnetic response M_y and M_z extracted from (a). (c) and (d) Identical energy scans at 2 K below T_c in the neutron SF channel and M_y , M_z , respectively. (e) The total neutron SF scattering σ_x^{SF} at 2 and 22 K and (f) their difference, where a neutron spin resonance is seen at $E_r = 7$ meV. (g) The σ_y^{SF} at 2 and 22 K and (h) their difference. (i),(j) Identical scans for σ_z^{SF} . The solid lines in (b),(d),(h),(j) are guides to the eyes, and in (f) the solid line is the sum of (h) and (j).

Figure 2(a) shows energy scans at $\mathbf{Q} = (0.5, 0.5, 3)$ for all three SF channels ($\sigma_\alpha^{\text{SF}}$) at $T = 22$ K. For a pure isotropic paramagnetic scattering, one expects $\sigma_x^{\text{SF}} = 2\sigma_y^{\text{SF}} = 2\sigma_z^{\text{SF}}$ assuming a small (negligible) background scattering [26,31]. While this is indeed the case for $E \geq 5$ meV, there is apparent spin anisotropy for $E < 5$ meV with $\sigma_y^{\text{SF}} > \sigma_x^{\text{SF}}/2 > \sigma_z^{\text{SF}}$ [Fig. 2(a)]. On cooling to $T = 2$ K, the spectra are rearranged [Fig. 2(c)]. While there is a clear resonance at $E_r \approx 7$ meV in the σ_x^{SF} channel at the expense of lower energy spin excitations [Fig. 2(e)], σ_y^{SF} and σ_z^{SF} respond to superconductivity very differently. Instead of showing suppressed spin fluctuations below 4 meV as in the temperature difference plot for σ_x^{SF} , superconductivity induces a very broad resonance in σ_y^{SF} with magnetic intensity gain from 3 to 10 meV [Figs. 2(g) and 2(h)]. This is similar to the c -axis polarized spin excitations of $\text{BaFe}_{1.9}\text{Ni}_{0.1}\text{As}_2$ below T_c [26] and $\text{BaFe}_{1.88}\text{Co}_{0.12}\text{As}_2$ [31]. For σ_z^{SF} , the effect of superconductivity is to open a larger spin gap below about 5 meV and form a resonance near $E_r = 7$ meV [Figs. 2(i) and 2(j)]. Since the temperature difference plots in

Figs. 2(f), 2(h), and 2(j) should contain no background, we expect $\sigma_x^{\text{SF}} = \sigma_y^{\text{SF}} + \sigma_z^{\text{SF}}$. The solid line in Fig. 2(f) shows the sum of σ_y^{SF} and σ_z^{SF} , and it is indeed statistically identical to σ_x^{SF} .

To quantitatively estimate the spin anisotropy from $\sigma_\alpha^{\text{SF}}$ in Figs. 2(a) and 2(c), we plot in Figs. 2(b) and 2(d) the energy dependence of M_y and M_z in the normal and superconducting states, respectively. At $T = 22$ K, the magnetic scattering show spin anisotropy below ~ 5 meV. At 2 K, the M_y shows a clean spin gap below 4 meV and a resonance at $E_r = 7$ meV, while M_z shows a broad peak centered around 5 meV. In previous polarized neutron scattering experiments on electron-doped iron pnictide superconductors [26,31], similar magnetic anisotropy was found at low energies.

Figure 3 summarizes constant energy scans along the $[H 1-H 3]$ direction at $E = 3$ and 7 meV with different neutron polarizations. At $T = 2$ K, σ_x^{SF} and σ_y^{SF} at $E = 3$ meV display well-defined peaks at (0.5, 0.5, 3) with almost the same magnitude, while σ_z^{SF} has only a broad weak peak center at (0.5, 0.5, 3) [Fig. 3(a)]. These data are consistent with constant- Q scans in Fig. 2. At $T = 22$ K, similar scans show three separate peaks satisfying $\sigma_y^{\text{SF}} > \sigma_x^{\text{SF}}/2 > \sigma_z^{\text{SF}}$, again confirming the anisotropic nature of the normal state spin excitations in Fig. 2(a). For comparison, spin excitations at the resonance energy of $E_r = 7$ meV are completely isotropic below [Fig. 3(c)] and above [Fig. 3(d)] T_c satisfying $\sigma_x^{\text{SF}} = 2\sigma_y^{\text{SF}} = 2\sigma_z^{\text{SF}}$.

Given the clear experimental evidence for anisotropic spin excitations at $E = 3$ meV and its possible coupling to superconductivity as illustrated in Figs. 2 and 3, it would be interesting to measure the temperature dependence of the spin anisotropy. Figure 4(a) shows the temperature dependent scattering for $\sigma_\alpha^{\text{SF}}$ at $\mathbf{Q} = (0.5, 0.5, 3)$ and $E = 3$ meV. At temperatures above 70 K, we see $\sigma_x^{\text{SF}} \approx 2\sigma_y^{\text{SF}} \approx 2\sigma_z^{\text{SF}}$ indicating that spin excitations are isotropic

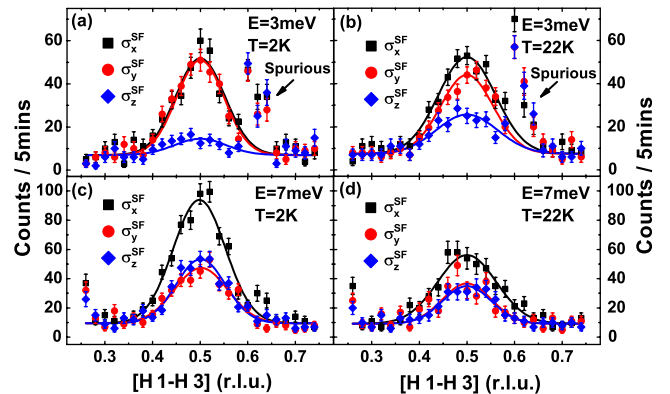


FIG. 3 (color online). (a),(b) Constant energy scans at 3 meV in the neutron SF channel $\sigma_{x,y,z}^{\text{SF}}$ below and above T_c , respectively. The solid lines are Gaussian fits to the data on linear backgrounds. (c) and (d) Identical scans and results at the resonance energy of $E_r = 7$ meV.

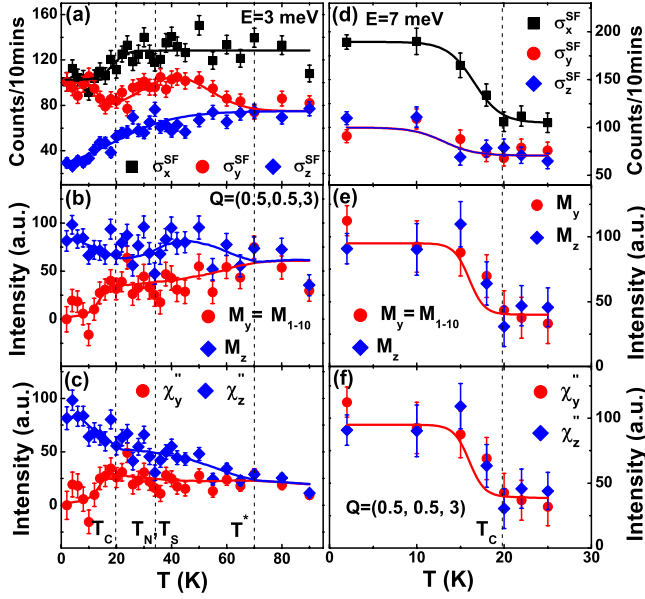


FIG. 4 (color online). (a) Temperature dependence of neutron SF scattering cross section $\sigma_{x,y,z}^{\text{SF}}$ at 3 meV and $\mathbf{Q} = (0.5, 0.5, 3)$. (b) The temperature dependence of magnetic response along the $[1\bar{1}0]$ (M_y) and $[11\bar{1}/3]$ (M_z) directions. Clear anisotropy persists up to $T^* = 70$ K. (c) Temperature dependence of the dynamic susceptibility, χ_y'' and χ_z'' . (d),(e),(f) Identical results at the resonance energy of $E_r = 7$ meV.

with $M_y = M_z$. On cooling to below 70 K, we see a clear splitting of the temperature dependent σ_y^{SF} and σ_z^{SF} . While σ_x^{SF} shows no visible changes cross 70 K, σ_y^{SF} increases and σ_z^{SF} decreases with decreasing temperature below 70 K before saturating around 40 K. On cooling further to crossing T_N and T_s , there are no statistically significant changes in σ_x^{SF} , σ_y^{SF} , or σ_z^{SF} , indicating that spin anisotropy at $E = 3$ meV does not respond to AFM ordering and tetragonal-orthorhombic lattice distortion. Finally, on cooling below T_c , we see a clear reduction in σ_x^{SF} , revealing a suppression of the spin excitations for energies below the resonance. On the other hand, while σ_y^{SF} increases at T_c and merges with σ_x^{SF} below around 10 K, σ_z^{SF} exhibits a further reduction in intensity below T_c . Figure 4(b) shows the temperature dependence of the magnetic scattering M_y and M_z obtained from $\sigma_\alpha^{\text{SF}}$. On cooling, spin excitations first change from isotropic to anisotropic below approximately 70 K, and further enhance anisotropy below T_c with almost zero M_y at 2 K. Figure 4(c) shows temperature dependence of the imaginary part of the dynamic susceptibility χ'' along the y and z directions. They show again the appearance of spin anisotropy below 70 K with no changes across T_N and T_s , and a further spin anisotropy change below T_c .

Figure 4(d) shows temperature dependence of the magnetic intensity at the resonance energy $E_r = 7$ meV. At all measured temperatures, we find $\sigma_x^{\text{SF}} \approx 2\sigma_y^{\text{SF}} \approx 2\sigma_z^{\text{SF}}$, thus confirming the isotropic nature of the mode. Figures 4(e) and 4(f) are the corresponding temperature dependence of

M_y , M_z and χ_y'' , χ_z'' , respectively. In both cases, there is an intensity increase below T_c , consistent with earlier work on the resonance [26,31]. For comparison, we note that spin excitations in superconducting iron chalcogenides have slightly anisotropic resonance with isotropic spin excitations below it [33,34].

In previous polarized neutron measurements on the parent compound BaFe_2As_2 [27], it was found that the in-plane polarized spin waves exhibit a larger gap than the out-of-plane polarized ones, suggesting that it costs more energy to rotate a spin within the orthorhombic a - b plane than to rotate it perpendicular to the FeAs layers. However, the spin anisotropy immediately disappears in the paramagnetic tetragonal state above T_N and T_s [27]. Since M_y is the spin moment in the FeAs layers [Fig. 1(e)], the M_y and M_z anisotropy should also represent the spin anisotropy along the $[1\bar{1}0]$ and $[11\bar{1}/3]$ directions, respectively. To determine the precise anisotropic direction of spin excitations at $E = 3$ meV, we measured $\sigma_\alpha^{\text{SF}}$ at $\mathbf{Q}_{1,2,3}$ in the (H, H, L) zone [Figs. 5(a)–5(c)]. At $T = 2$ K ($\ll T_c$), we see $\sigma_x^{\text{SF}} \approx \sigma_z^{\text{SF}} \gg \sigma_y^{\text{SF}}$ at all wave vectors probed. On warming to 35 K ($> T_N, T_s$), we have $\sigma_x^{\text{SF}} > \sigma_z^{\text{SF}} > \sigma_y^{\text{SF}}$. At 75 K, we find $\sigma_x^{\text{SF}} \approx 2\sigma_y^{\text{SF}} \approx 2\sigma_z^{\text{SF}}$, suggesting weak or no spin anisotropy. By considering wave vector dependence of spin excitations in Figs. 5(a)–5(c), we estimate the temperature dependence of M_{110} , $M_{1\bar{1}0}$, and M_{001} [Fig. 5(d)] (see Supplemental Material [35]).

In the superconducting orthorhombic state, there are clear in-plane magnetic anisotropy with $M_{001} \sim M_{110} \gg M_{1\bar{1}0} \approx 0$. In the paramagnetic tetragonal state just above T_s and T_N , we still have strong in-plane magnetic anisotropy with $M_{110} \sim M_{001} > M_{1\bar{1}0}$. This is surprising because domains associated with the in-plane AFM wave vector $\mathbf{Q} = (0.5, 0.5)$ are randomly mixed with those associated

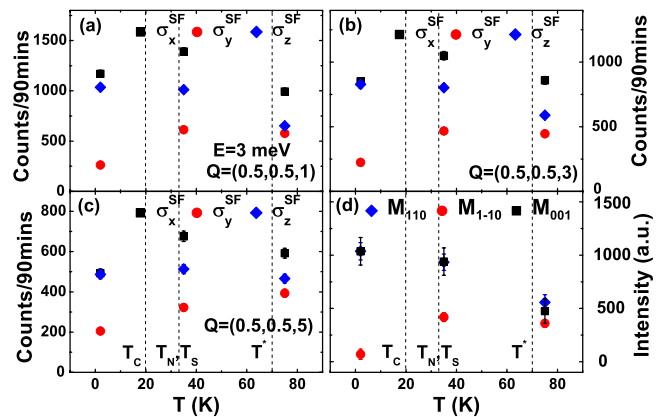


FIG. 5 (color online). (a)–(c) Temperature dependence of neutron SF scattering cross section $\sigma_{x,y,z}^{\text{SF}}$ at 3 meV and $\mathbf{Q}_{1,2,3} = (0.5, 0.5, L)$ with $L = 1, 3, 5$. (d) The temperature dependence of magnetic response along the $[110]$ (M_{110}), $[1\bar{1}0]$ ($M_{1\bar{1}0}$), and $[001]$ (M_{001}) directions. Clear in-plane anisotropy persists up to $T^* = 70$ K.

with the $\mathbf{Q} = (0.5, -0.5)$ in the tetragonal phase. In the AFM orthorhombic state, the low-energy spin excitations associated with the $\mathbf{Q} = (0.5, 0.5)$ domains are well separated from those associated with $\mathbf{Q} = (0.5, -0.5)$ in reciprocal space [11]. If there is strong paramagnetic scattering at $\mathbf{Q} = (0.5, -0.5)$ arising from domains associated with $\mathbf{Q} = (0.5, 0.5)$ in the tetragonal phase, one should not be able to determine the spin excitation anisotropy in neutron polarization analysis. However, recent unpolarized neutron experiments on nearly 100% mechanically detwinned $\text{BaFe}_{2-x}\text{Ni}_x\text{As}_2$ reveal that spin excitations in the paramagnetic tetragonal state are still centered mostly at $\mathbf{Q} = (0.5, 0.5)$ [36]. Therefore, our neutron polarization analysis provides the most compelling evidence for the in-plane spin anisotropy in the paramagnetic tetragonal phase of $\text{BaFe}_{1.904}\text{Ni}_{0.096}\text{As}_2$ [Fig. 5(d)]. Since such spin excitation anisotropy occurs at the AFM wave vector $\mathbf{Q} = (0.5, 0.5)$, it does not break the C_4 rotational symmetry of the underlying lattice.

In summary, we have discovered that an in-plane isotropic-to-anisotropic spin fluctuation transition occurs in the tetragonal phase of superconducting $\text{BaFe}_{1.904}\text{Ni}_{0.096}\text{As}_2$ without an uniaxial pressure, consistent with resistivity anisotropy. The spin anisotropy is further enhanced upon entering into the superconducting state. Therefore, our experimental results establish the in-plane spin anisotropy as a new experimental probe to study the spontaneously broken electronic symmetries in strain free iron pnictides.

The work at IOP, CAS, is supported by MOST (973 Projects No. 2012CB821400, No. 2011CBA00110, and No. 2010CB833102) and NSFC (No. 11004233). The work at UTK and Rice University is supported by the U.S. NSF, Contract No. NSF-DMR-1063866 and No. NSF-OISE-0968226.

*pdai@rice.edu

- [1] E. Fradkin, S. A. Kivelson, M. J. Lawler, J. P. Eisenstein, and A. P. Mackenzie, *Annu. Rev. Condens. Matter Phys.* **1**, 153 (2010).
- [2] Y. Kamihara, T. Watanabe, M. Hirano, and H. Hosono, *J. Am. Chem. Soc.* **130**, 3296 (2008).
- [3] C. de la Cruz *et al.*, *Nature (London)* **453**, 899 (2008).
- [4] P. C. Dai, J. P. Hu, and E. Dagotto, *Nat. Phys.* **8**, 709 (2012).
- [5] J. Zhao, D. T. Adroja, D. X. Yao, R. Bewley, S. L. Li, X. F. Wang, G. Wu, X. H. Chen, J. P. Hu, and P. C. Dai, *Nat. Phys.* **5**, 555 (2009).
- [6] T.-M. Chuang, M. P. Allan, J. Lee, Y. Xie, N. Ni, S. L. Bud'ko, G. S. Boebinger, P. C. Canfield, and J. C. Davis, *Science* **327**, 181 (2010).
- [7] T. Shimojima *et al.*, *Phys. Rev. Lett.* **104**, 057002 (2010).
- [8] I. R. Fisher, L. Degiorgi, and Z. X. Shen, *Rep. Prog. Phys.* **74**, 124506 (2011).
- [9] R. M. Fernandes, L. H. VanBebber, S. Bhattacharya, P. Chandra, V. Keppens, D. Mandrus, M. A. McGuire, B. C. Sales, A. S. Sefat, and J. Schmalian, *Phys. Rev. Lett.* **105**, 157003 (2010).
- [10] M. Yi *et al.*, *Proc. Natl. Acad. Sci. U.S.A.* **108**, 6878 (2011).
- [11] L. W. Harriger, H. Q. Luo, M. S. Liu, C. Frost, J. P. Hu, M. R. Norman, and P. C. Dai, *Phys. Rev. B* **84**, 054544 (2011).
- [12] S. Kasahara, H. J. Shi, K. Hashimoto, S. Tonegawa, Y. Mizukami, T. Shibauchi, K. Sugimoto, T. Fukuda, T. Terashima, A. H. Nevidomskyy, and Y. Matsuda, *Nature (London)* **486**, 382 (2012).
- [13] J. P. Hu and C. K. Xu, *Physica (Amsterdam)* **481C**, 215 (2012).
- [14] C. C. Lee, W. G. Yin, and W. Ku, *Phys. Rev. Lett.* **103**, 267001 (2009).
- [15] F. Krüger, S. Kumar, J. Zaanen, and J. van den Brink, *Phys. Rev. B* **79**, 054504 (2009).
- [16] W. C. Lv, J. S. Wu, and P. Phillips, *Phys. Rev. B* **80**, 224506 (2009).
- [17] M. Daghofer, Q. L. Luo, R. Yu, D. X. Yao, A. Moreo, and E. Dagotto, *Phys. Rev. B* **81**, 180514(R) (2010).
- [18] C.-C. Chen, J. Maciejko, A. P. Sorini, B. Moritz, R. R. P. Singh, and T. P. Devereaux, *Phys. Rev. B* **82**, 100504(R) (2010).
- [19] B. Valenzuela, E. Bascones, and M. J. Calderón, *Phys. Rev. Lett.* **105**, 207202 (2010).
- [20] M. Nakajima, S. Ishida, Y. Tomioka, K. Kihou, C. H. Lee, A. Iyo, T. Ito, T. Kakeshita, H. Eisaki, and S. Uchida, *Phys. Rev. Lett.* **109**, 217003 (2012).
- [21] C. Dhital, Z. Yamani, W. Tian, J. Zeretsky, A. S. Sefat, Z. Wang, R. J. Birgeneau, and S. D. Wilson, *Phys. Rev. Lett.* **108**, 087001 (2012).
- [22] S. Ishida, M. Nakajima, T. Liang, K. Kihou, C. H. Lee, A. Iyo, H. Eisaki, T. Kakeshita, Y. Tomioka, T. Ito, and S. Uchida, *Phys. Rev. Lett.* **110**, 207001 (2013).
- [23] M. P. Allan, T.-M. Chuang, F. Massee, Y. Xie, N. Ni, S. L. Bud'ko, G. S. Boebinger, Q. Wang, D. S. Dessau, P. C. Canfield, M. S. Golden, and J. C. Davis, *Nat. Phys.* **9**, 220 (2013).
- [24] H. Q. Luo, R. Zhang, M. Laver, Z. Yamani, M. Wang, X. Y. Lu, M. Y. Wang, Y. C. Chen, S. L. Li, S. Chang, J. W. Lynn, and P. C. Dai, *Phys. Rev. Lett.* **108**, 247002 (2012).
- [25] X. Y. Lu, H. Gretarsson, R. Zhang, X. R. Liu, H. Q. Luo, W. Tian, M. Laver, Z. Yamani, Y.-J. Kim, A. H. Nevidomskyy, Q. Si, and P. C. Dai, *Phys. Rev. Lett.* **110**, 257001 (2013).
- [26] O. J. Lipscombe, L. W. Harriger, P. G. Freeman, M. Enderle, C. L. Zhang, M. Y. Wang, T. Egami, J. P. Hu, T. Xiang, M. R. Norman, and P. C. Dai, *Phys. Rev. B* **82**, 064515 (2010).
- [27] N. Qureshi, P. Steffens, S. Wurmehl, S. Aswartham, B. Büchner, and M. Braden, *Phys. Rev. B* **86**, 060410(R) (2012).
- [28] Y. C. Chen, X. Y. Lu, M. Wang, H. Q. Luo, and S. L. Li, *Supercond. Sci. Technol.* **24**, 065004 (2011).
- [29] H.-H. Kuo, J.-H. Chu, S. C. Riggs, L. Yu, P. L. McMahon, K. De Greve, Y. Yamamoto, J. G. Analytis, and I. R. Fisher, *Phys. Rev. B* **84**, 054540 (2011).

- [30] S. Nandi, M. G. Kim, A. Kreyssig, R. M. Fernandes, D. K. Pratt, A. Thaler, N. Ni, S. L. Bud'ko, P. C. Canfield, J. Schmalian, R. J. McQueeney, and A. I. Goldman, *Phys. Rev. Lett.* **104**, 057006 (2010).
- [31] P. Steffens, C. H. Lee, N. Qureshi, K. Kihou, A. Iyo, H. Eisaki, and M. Braden, *Phys. Rev. Lett.* **110**, 137001 (2013).
- [32] M. S. Liu, C. Lester, J. Kulda, X. Y. Lu, H. Q. Luo, M. Wang, S. M. Hayden, and P. C. Dai, *Phys. Rev. B* **85**, 214516 (2012).
- [33] P. Babkevich, B. Roessli, S. N. Gvasaliya, L.-P. Regnault, P. G. Freeman, E. Pomjakushina, K. Conder, and A. T. Boothroyd, *Phys. Rev. B* **83**, 180506(R) (2011).
- [34] K. Prokeš, A. Hiess, W. Bao, E. Wheeler, S. Landsgesell, and D. N. Argyriou, *Phys. Rev. B* **86**, 064503 (2012).
- [35] See Supplemental Material at <http://link.aps.org/supplemental/10.1103/PhysRevLett.111.107006> for details on how to estimate M_{110} , $M_{1\bar{1}0}$, and M_{001} .
- [36] X. Y. Lu *et al.* (unpublished).